Chapter 3
Particle Acceleration Mechanisms

Rami Vainio and Alexandr Afanasiev

Abstract This chapter provides a short tutorial review on particle acceleration in dynamic electromagnetic fields under scenarios relevant to the problem of particle acceleration in the solar corona and solar wind during solar eruptions. It concentrates on fundamental aspects of the acceleration process and refrains from presenting detailed modeling of the specific conditions in solar eruptive plasmas. All particle acceleration mechanisms (in the solar corona) are related to electric fields that can persist in the highly conductive plasma: either electrostatic (or potential) or inductive related to temporally variable magnetic fields through Faraday's law. Mechanisms involving both kinds of fields are included in the tutorial.

3.1 Introduction

Solar energetic particles (SEPs) are accelerated in flares and coronal mass ejections (CMEs) (see Chap. 2 and references therein). In this chapter, we will give a tutorial review of particle acceleration mechanisms in solar eruptions. The aim is not to give a comprehensive review of the original literature but rather give the reader an idea of what are the main ideas that could explain the acceleration of ions and electrons to the relativistic energies, we observe to be produced in the SEP events. For recent reviews on SEPs we direct the reader to Desai and Giacalone (2016) and Reames (2017).

SEPs are accelerated in the electromagnetic fields related to the dynamics of the solar corona and solar wind during solar eruptions. In quasi-static fields of the quiet-time solar corona, strong electric fields would not exist and particle acceleration beyond quasi-thermal energies (up to ∼keV) would seldom occur. However, solar eruptions are manifestations of very non-thermal conditions favorable for particle acceleration.

Magnetic reconnection is by definition a process, which requires electric fields to be present in the system. As discussed in Chap. 2 the plasma advected towards

R. Vainio (✉) • A. Afanasiev
Department of Physics and Astronomy, University of Turku, Turku, Finland
e-mail: rami.vainio@utu.fi; alexandr.afanasiev@utu.fi

O.E. Malandraki, N.B. Crosby (eds.), *Solar Particle Radiation Storms Forecasting and Analysis, The HESPERIA HORIZON 2020 Project and Beyond*, Astrophysics and Space Science Library 444, DOI 10.1007/978-3-319-60051-2_3

a current sheet with a frozen-in magnetic field will be associated with a convective electric field, which can accelerate particles. The situation is most likely a dynamic one, where induced electric fields with closed field lines will be generated by temporally varying magnetic fields. As discussed in Sect. 3.2.1, this can lead to very efficient conditions for particle acceleration. Reconnection outflows from the corona towards the Sun may generate collapsing loop systems, which can also act as particle accelerators. In addition to direct acceleration by large scale fields, reconnection jets in flares can also be turbulent regions. These can give rise to stochastic acceleration in the plasma (see Sect. 3.2.5). Even shock acceleration (Sect. 3.2.3) could in principle occur in reconnection regions, since the super-Alfvénic reconnection jets can be terminated by dense plasma or strong magnetic fields impeding their flow. Flares are commonly thought of as being the source of (at least) the impulsive SEP events (Reames 2017). These events show peculiar abundance ratios of ions difficult to explain in terms of non-selective acceleration processes, as shock acceleration. Presently the abundances are probably best explained by stochastic acceleration (Petrosian 2012).

Especially the gradual SEP events are undoubtedly related to CMEs. Mostly, but not exclusively, because of the morphology of the time-intensity profiles of the MeV and deka-MeV protons, showing clear organization based on the magnetic connectivity of the observer to the CME, the bow shock driven by the fast magnetized eruption has been identified as the prime candidate for accelerating the ions in SEP gradual events (Desai and Giacalone 2016; Reames 2017). There is a large amount of evidence that CME-driven shocks accelerate protons up to some tens of MeVs, but the case becomes more open at energies approaching and exceeding 100 MeV. Theoretical modeling (see, e.g., Chap. 9), however, suggests that CME-driven shocks are able to accelerate ions also to relativistic energies. For electrons, strong correlation between the observed flux properties of deka-MeV protons and MeV electrons (see, e.g., Chap. 7) could point towards shock acceleration as well, but the theoretical foundations of electron acceleration by shocks are not on such solid basis as for ions, mainly because electrons resonate with plasma fluctuations at much lower scales than protons (see Sect. 3.2.2). The main shock acceleration mechanisms are, however, able to accelerate electrons as well. In addition to shock acceleration, the CME downstream region hosts regions of strong plasma compression and turbulence. Such regions may accelerate particles via the compressional acceleration mechanism (Sect. 3.2.4) and stochastically (Sect. 3.2.5), respectively. Note also, that coronal magnetic restructuring (outside the flaring active region) behind the CME may also lead to particle acceleration via many of the same mechanisms.

3.2 Acceleration Mechanisms

Particle acceleration in solar plasmas requires electric fields and the ability of particles to propagate along them, since the energy gain rate produced by the

Lorentz force, $q(\mathbf{E} + \mathbf{v} \times \mathbf{B})$, is $\dot{W} = q\mathbf{v} \cdot \mathbf{E}$. Here q, $\mathbf{v}$, and W are the charge, the velocity and the kinetic energy of the particle and $\mathbf{E}$ and $\mathbf{B}$ are the electric and the magnetic field. Electric fields can be derived from the scalar and vector potential of the electromagnetic field:

$$\mathbf{E} = -\nabla\phi - \frac{\partial \mathbf{A}}{\partial t}, \tag{3.1}$$

and the magnetic field from the vector potential $\mathbf{B} = \nabla \times \mathbf{A}$. Particles can move in the direction of the electric field in several possible ways. In the following, we will discuss the different possibilities briefly.

3.2.1 *Large-Scale Electric Field Acceleration*

We will first discuss electric fields in large scales, meaning that the field changes over scales that are large compared to the gyroradii of the accelerated particles. In the simplest case, the electric field has a component parallel to the magnetic field, along which ions and electrons can move without being affected by the magnetic field. Large-scale, static parallel electric fields are, however, not easy to set up in dilute coronal plasmas, since in the near absence of collisions, electrons can usually move very quickly along the magnetic field and build up charge separation to counter any accelerating parallel electric field. In the presence of magnetic field inhomogeneities, however, gradient and curvature drifts can move ions and electrons in the direction perpendicular to the field. This may lead to particles gaining energy, if there is an electric field along the direction of the drift motion. This is the basis of several shock-acceleration mechanisms to be discussed in Sect. 3.2.3.

Magnetic reconnection is perhaps the most obvious plasma process to set up large-scale electric fields. Some models consider static electric fields accelerating particles near magnetic nulls, where particles can propagate along the electric field unimpeded (Litvinenko 1996). This, however, is not the only way to set up a large scale electric field that particles can utilize effectively to get accelerated.

Choosing to work in the Coulomb cauge ($\nabla \cdot \mathbf{A} = 0$), the electric fields due to charge separation are all described by the scalar potential and, thus,

$$\nabla^2\phi = -\frac{\rho_q}{\epsilon_0}. \tag{3.2}$$

Therefore, the part of the electric field related to the vector potential contains inductive fields related to the time derivative of the magnetic field via Faraday's law. These electric fields are then described by fields lines that are either closed loops or extend to the boundaries of the system. Electric fields induced by the temporally variable magnetic field (or vector potential) can sometimes lead to very efficient acceleration of particles. Let us illustrate this with an example.

Consider

$$\mathbf{B} = B_0 \left(\frac{y\mathbf{e}_x - x\mathbf{e}_y}{r_0} + \gamma_0 t \mathbf{e}_z \right) = \nabla \times \mathbf{A} \tag{3.3}$$

$$\mathbf{A} = B_0 \left(-\frac{y\mathbf{e}_x - x\mathbf{e}_y}{2} \gamma_0 t + \frac{x^2 + y^2}{2r_0} \mathbf{e}_z \right), \quad \nabla \cdot \mathbf{A} = 0 \tag{3.4}$$

$$\mu_0 \mathbf{J} = \nabla \times \mathbf{B} = -\frac{2B_0}{r_0} \mathbf{e}_z \tag{3.5}$$

This magnetic configuration is represented by a helical magnetic field, where the axial field increases linearly with time and the poloidal field (driven by a constant axial current) is constant (see Fig. 3.1).

The axial magnetic field is generated by a poloidal external current flying at some radial distance, e.g., $r = r_0$, increasing linearly with time. We neglect the displacement current so the time evolution of the axial field (and external current) has to be slow in the sense that $r_0 \gamma_0 \ll c$. With these assumptions, the induced electric field is

$$\mathbf{E} + \nabla \phi = -\frac{\partial \mathbf{A}}{\partial t} = \gamma_0 B_0 \frac{y\mathbf{i} - x\mathbf{j}}{2} = \tfrac{1}{2} r_0 \gamma_0 \mathbf{B}_\mathrm{p}. \tag{3.6}$$

Clearly, the induced electric field is in the direction of the poloidal magnetic field and, therefore, particles propagating along the field lines will be accelerated along the field, ions in one direction and electrons in the other. The axial field, however, will make sure that electrons and ions will also propagate along the axial direction,

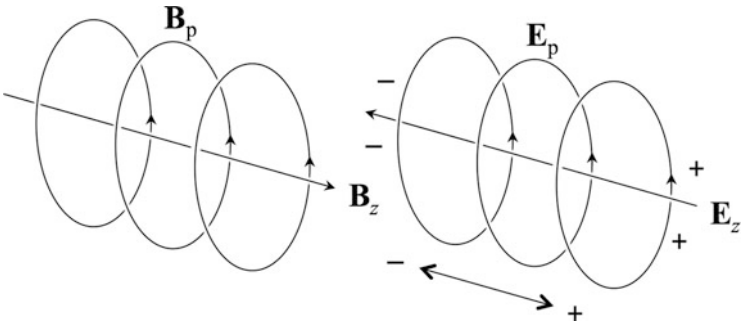

Fig. 3.1 Electromagnetic fields in the simple model. The magnetic field (*left*) is a helix, where the axial field ($\mathbf{B}_z$) is linearly increasing with time and the poloidal field ($\mathbf{B}_\mathrm{p}$) is driven by a homogeneous axial current. The poloidal electric field $\mathbf{E}_\mathrm{p}$ (*right*) is induced by the time-dependent axial magnetic field and it is in the same direction as the poloidal magnetic field. Charge separation caused by the particles accelerated by $\mathbf{E}_\mathrm{p}$ along the magnetic field lines will produce an oppositely directed axial electric field. This would eventually turn the electric field perpendicular to the magnetic field if charge separation is let to build up in the plasma

in the opposite directions. Thus, charge separation will be set up. It produces a potential field in the axial and radial direction, which combined to the induced field could produce a total electric field perpendicular to the magnetic field. The condition would be

$$\mathbf{E}\cdot\mathbf{B} = \frac{r^2\gamma_0}{2r_0}B_0^2 - B_0\gamma_0 t\frac{\partial\phi}{\partial z} \sim 0$$

$$\Rightarrow \phi \sim \frac{r^2 z B_0}{2r_0 t} \quad \Rightarrow -\nabla\phi \sim -\frac{rzB_0}{r_0 t}\mathbf{e}_r - \frac{r^2 B_0}{2r_0 t}\mathbf{e}_z \tag{3.7}$$

However, it is clear that this field can be approached only after a finite time (as it diverges at $t \to 0$). Thus, during a limited amount of time, the induced electric field can accelerate particles very efficiently.

We notice also that particles could be accelerated by the induced electric field even without the poloidal magnetic field in the system. If only the axial magnetic field is present, particles will perform gyro-motion around it. The contour integral of the Lorentz force along one circular Larmor orbit,

$$\Delta W_\perp = \oint_{\mathrm{L}} q\mathbf{E}\cdot\mathrm{d}\mathbf{l}, \tag{3.8}$$

is in the left-handed [right-handed] sense around the magnetic field $\mathbf{B} = B(t)\,\mathbf{e}_z$ for $q > 0$ [$q < 0$]. Taking the integral in the right-handed sense (denoted below by the minus sign after L) gives

$$\begin{aligned}\Delta W_\perp &= -|q|\oint_{\mathrm{L}-}\mathbf{E}\cdot\mathrm{d}\mathbf{l} = -|q|\int_{A_\mathrm{L}}(\nabla\times\mathbf{E})\cdot(\mathbf{e}_z\,\mathrm{d}S)\\ &= |q|\int_{A_\mathrm{L}}\frac{\partial\mathbf{B}}{\partial t}\cdot(\mathbf{e}_z\,\mathrm{d}S) = |q|\pi r_\mathrm{L}^2\frac{\partial B}{\partial t}\end{aligned} \tag{3.9}$$

Since the Larmor radius is $r_\mathrm{L} = v_\perp\tau_\mathrm{L}/2\pi$, where $\tau_\mathrm{L} = 2\pi\gamma m/|q|B$ is the particle gyrotime, and γ and m its Lorentz factor and mass, respectively, we have

$$\begin{aligned}v_\perp\Delta p_\perp &= \Delta W_\perp = |q|\pi\frac{v_\perp\tau_\mathrm{L}}{2\pi}\frac{\gamma m v_\perp}{|q|B}\frac{\partial B}{\partial t}\\ \Rightarrow \frac{\dot{p}_\perp}{p_\perp} &= \frac{1}{p_\perp}\frac{\Delta p_\perp}{\tau_\mathrm{L}} = \frac{1}{2B}\frac{\partial B}{\partial t} = \tfrac{1}{2}\gamma_0,\end{aligned} \tag{3.10}$$

which describes the betatron acceleration process. Clearly, $p_\perp = p_{\perp 0}\mathrm{e}^{\frac{1}{2}\gamma_0 t}$ gives the perpendicular particle momentum in terms of its initial value $p_{\perp 0}$ at $t = 0$.

3.2.2 Resonant Wave Acceleration

As discussed above, generating electric fields with quasi-static components along the magnetic field is not easy. Instead of large scale fields, the fields can also be at the gyromotion scale, and such fields can be carried by various plasma waves. At first sight, if the electric field is fluctuating, it is quasi-periodically pointing in opposite directions and the time integral of the acceleration would seem to vanish in most cases. In this case, however, it is possible for the particle to be in resonance with the wave's electric field: if the period of particle motion agrees with the period of the wave, the phase of the wave at the location of the particle can be constant, leading to a constant accelerating electric field felt by the particle.

This process can be illustrated with a simple linearized model. Consider the electric field of a circularly polarized wave propagating along the mean magnetic field taken to be constant and along the z axis. Thus,

$$\mathbf{E}_1 = E_1[\mathbf{e}_x \cos(kz - \omega t) - \mathbf{e}_y \sin(kz - \omega t)], \tag{3.11}$$

and the phase speed of the wave is $V_\phi = \omega/k$. The electric and magnetic fields of the wave are related via Faraday's law, i.e.,

$$\begin{aligned} \frac{\partial \mathbf{B}_1}{\partial t} &= -\nabla \times \mathbf{E}_1 = -\begin{vmatrix} \mathbf{e}_x & \mathbf{e}_y & \mathbf{e}_z \\ \partial_x & \partial_y & \partial_z \\ E_{1x} & E_{1y} & 0 \end{vmatrix} = \mathbf{e}_x \frac{\partial E_{1y}}{\partial z} - \mathbf{e}_y \frac{\partial E_{1x}}{\partial z} \\ &= kE_1[-\mathbf{e}_x \sin(kz - \omega t) - \mathbf{e}_y \cos(kz - \omega t)] \end{aligned} \tag{3.12}$$

$$\Rightarrow \mathbf{B}_1 = \frac{k}{\omega} E_1[-\mathbf{e}_x \cos(kz - \omega t) + \mathbf{e}_y \sin(kz - \omega t)] \tag{3.13}$$

$$\Rightarrow \mathbf{E}_1 = -\frac{\omega}{k}\mathbf{B}_1 = -V_\phi \mathbf{B}_1, \tag{3.14}$$

i.e., the magnetic field is circularly polarized, as well. In case the phase speed is less than the speed of light, we can always make a boost along the z axis to a coordinate system where the wave frequency is zero. In this frame the wave electric field vanishes and the charged particles interacting with the wave conserve their energy. In the laboratory frame the change in the particle energy is, thus, obtained through

$$\Delta W = \Gamma_\phi V_\phi p' \Delta\mu', \tag{3.15}$$

where $\Gamma_\phi = (1 - V_\phi^2/c^2)^{-1/2}$, μ' and p' are the pitch-angle cosine and the (constant) momentum magnitude of the particle in the wave frame, and ΔX represents the

change in the quantity X. The equations of motion in the wave frame (omitting the primes) can be written as

$$\dot{\mu} = \frac{B_1}{B_0}\sqrt{1-\mu^2}\Omega_0 \cos(\varphi + kz) \tag{3.16}$$

$$\dot{\varphi} = -\Omega_0 + \frac{B_1}{B_0}\frac{\mu}{\sqrt{1-\mu^2}}\Omega_0 \sin(\varphi + kz) \tag{3.17}$$

$$\dot{z} = v\mu, \tag{3.18}$$

where φ is the phase angle measured around the z axis and $\Omega_0 = qB_0/\gamma m$ is the particle's relativistic (signed) gyro-frequency. Now, assuming that the magnetic amplitude of the wave is small compared to the mean magnetic field, $B_1 \ll B_0$, we can approximate the phase angle evolution by $\varphi = \varphi_0 - \Omega_0 t$. Substituting that to the equation for μ shows a resonance (a constant right-hand side) at $kz - \Omega_0 t = 0$

$$\Rightarrow kv\mu = \Omega_0, \tag{3.19}$$

which is the cyclotron resonance condition between charged particles and electromagnetic waves propagating parallel to the mean magnetic field, written in the rest-frame of the wave. Transforming back to the laboratory frame gives the resonance condition as

$$\omega - kv\mu = -\Omega_0, \tag{3.20}$$

where negative (positive) frequencies denote left-handed (right-handed) polarization. The circular polarization of the wave has to match the handedness of the particle motion in the guiding-centre rest-frame (where $v\mu = 0$), so ions (electrons) resonate with left-hand (right-hand) polarized waves in that frame. The wave-particle resonance is sketched for protons and cold-plasma waves in Fig. 3.2. We can see that low-energy protons (with $|v\mu| \lesssim 2V_\mathrm{A}$) can only resonate with counter-propagating left-handed waves (Vainio 2000).

Approximating the left-handed dispersion curve with a straight line at $-\Omega_0 < \omega < 0$ simplifies the picture so that the phase speed of the resonant wave is constant. Thus, the relevant wave-frame, where the proton would conserve its energy, is propagating at speed $\pm V_\mathrm{A}$ along the background field and protons with positive [negative] parallel speed resonate with waves with $\omega/k_\parallel = -V_\mathrm{A}$ [$\omega/k_\parallel = +V_\mathrm{A}$]. Thus, their position in $(v_\parallel, v_\perp)$ velocity plane is constrained on semicircles centered at $v_\parallel = \pm V_\mathrm{A}$. Starting from low speeds, $v_0 \ll V_\mathrm{A}$, wave-frame pitch-angle scattering leads to an increase of perpendicular velocity of protons, as depicted in Fig. 3.3. If the extent of the initial distribution in the parallel direction is v_0, then the extent of the final distribution in the perpendicular direction would be

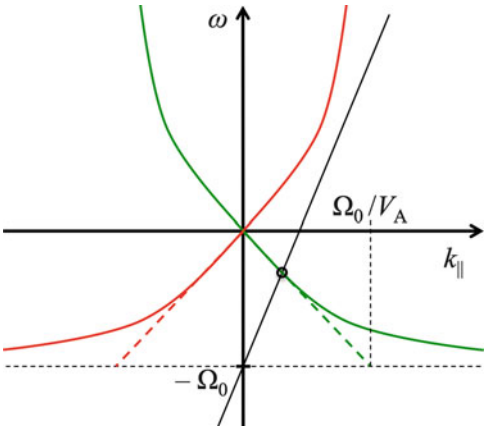

Fig. 3.2 Cyclotron resonance of protons with parallel propagating cold-plasma waves. The resonance condition, Eq. (3.19), is depicted with the *black line* for a proton with positive parallel speed $v\mu$. The *green and the red curves* give the dispersion relations of parallel-propagating cold-plasma waves with negative frequencies denoting the left-handed Alfvén–ion-cyclotron waves and positive frequencies the right-handed fast-MHD–whistler waves. The *red (green) line* gives the wave with positive (negative) phase speed $\omega/k_\parallel$. The *red (green) dashed lines* depict the low-frequency approximation to the dispersion relation, i.e., the Alfvén waves with positive (negative) phase speed, $\omega/k_\parallel = \pm V_\mathrm{A}$. The wave-particle resonances are found where the *black line* crosses the dispersion curves

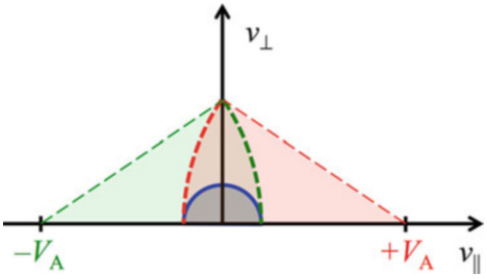

Fig. 3.3 The resonant-wave acceleration process. Particles are scattered off electromagnetic waves propagating in the medium at phase speeds $\pm V_\phi$, here approximated with $\pm V_\mathrm{A}$. Scattering is elastic in the wave frame, which leads to particles conserving their kinetic energies in that frame. If waves have left-handed polarization, low-energy ions resonate with them when propagating in the opposite direction (in the plasma frame) than the wave. Particles initially in the *grey region* inside the *blue semi-circle* will be scattered by the waves to fill the intersection of the *green and red sectors*, centered at $v_\parallel = -V_\mathrm{A}$ and $v_\parallel = +V_\mathrm{A}$, respectively

$\sqrt{(V_\mathrm{A} + v_0)^2 - V_\mathrm{A}^2} = \sqrt{2V_\mathrm{A}v_0 + v_0^2}$ and the ratio of final perpendicular and initial parallel energies is

$$\frac{W_{\perp,\max}}{W_{\parallel,0}} = \frac{v_0^2 + 2V_\mathrm{A}v_0}{v_0^2} = 1 + \frac{2V_\mathrm{A}}{v_0}, \tag{3.21}$$

so obviously the mechanism alone cannot accelerate ions to very high energies. This mechanism is, however, the basis of the cyclotron heating models of the solar corona (Isenberg 2001).

The resonant wave-acceleration process in solar flares is thought to be responsible for the preferential acceleration of minor ions. The dispersion relations of the waves in a multi-species plasma are not as simple as in Fig. 3.2, but contain additional resonances ($|k_\parallel| \to \infty$) with thermal He^4 ions at cyclotron frequency half of protons, $\Omega_\alpha = \frac{1}{2}\Omega_p$. Ions with cyclotron frequencies differing from that of protons and alpha particles are much more efficiently accelerated than protons and alphas in such plasmas. We will come back to this in Sect. 3.2.5.

3.2.3 Shock Acceleration

Shocks can accelerate particles in various ways. The three most commonly studied mechanisms are shock drift acceleration (SDA), shock surfing acceleration and diffusive shock acceleration (DSA).

SDA occurs, when a particle interacts once with a quasi-perpendicular shock front (Fig. 3.4, panels a and b) (Sarris and Van Allen 1974). The particle drifts (due to the motional electric field, $\mathbf{E} = -\mathbf{u}_1 \times \mathbf{B}_1$) with the upstream bulk speed u_{1x} toward the shock wave. When the ion [electron] hits the shock front, it feels the stronger downstream magnetic field, meaning that its Larmor radius is smaller than in the upstream field, and that its guiding center shifts parallel [anti-parallel] to the electric field. Thus, the particle is accelerated. During their interaction with the shock the particles, at least in an averaged sense, conserve their first adiabatic invariant, $p_\perp^2/B$. For a perpendicular shock, we then get

$$\frac{p_2^2}{B_2} = \frac{p_1^2}{B_1} \quad \Rightarrow \quad p_2 = p_1\sqrt{\frac{B_2}{B_1}}, \tag{3.22}$$

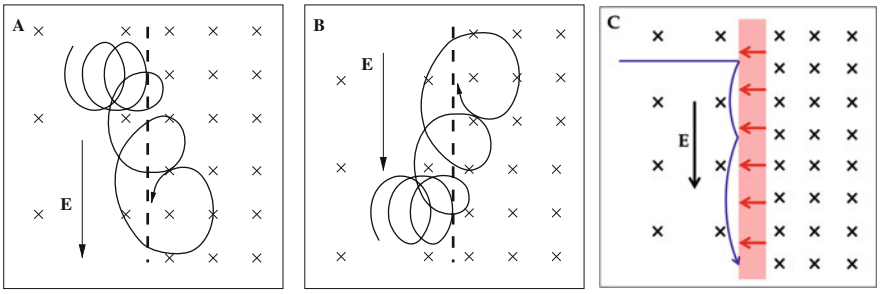

Fig. 3.4 Shock drift acceleration and shock surfing. An energetic charged particle is convected to a quasi-perpendicular shock from upstream by the electric-field drift. In the shock front, due to magnetic field gradient in the front, (**a**) ions drift parallel and (**b**) electrons drift anti-parallel to the electric field and, thus, gain energy. Panel (**c**) depicts an ion surfing on the shock due to multiple reflections by the cross-shock potential electric field. (Panels (**a**) and (**b**) from Koskinen 2011)

so the particle momentum in the downstream region, p_2, is approximately $\sqrt{B_2/B_1}$ times the particle momentum in the upstream region, p_1. The total gain in energy is, therefore, not very significant, but may explain the so-called shock spike events observed during nearly perpendicular interplanetary shocks crossing the spacecraft.

SDA operates in oblique shocks as well, but slightly modified. It is most advantageous to transform to the so-called de Hoffmann–Teller frame, where the flow and the magnetic field are parallel throughout the shock and the motional electric field vanishes. This transformation from the upstream plasma frame is along the magnetic field at speed $u_1 = u_{1x}/\cos\Theta_{\mathrm{Bn}}$ away from the shock in the upstream region. Here Θ_{Bn} is the shock normal angle. Now, particles incident on the shock from the upstream side with high-enough pitch-angle, i.e., with $1-\mu^2 > B_1/B_2$, cannot enter the downstream side of the shock while conserving their adiabatic invariant and, thus, are reflected back to the upstream region. This reflection process, when viewed in the upstream plasma frame, give the reflected particle a parallel momentum addition of the same order as transmission in the quasi-perpendicular shock.

Shock surfing (Fig. 3.4, panel c) is related to SDA in the sense that the accelerating electric field is the same, the motional electric field. However, the drift motion along the field is related to the upstream-directed cross-shock potential electric field, caused by charge separation at the shock front (Shapiro and Üçer 2003). The cross-shock potential electric field can specularly reflect ions incident on the shock and enable their acceleration in the direction of the motional electric field. The specular reflections can occur multiple times at a grazing angle. This leads to ion trajectories surfing on the shock front in the direction of the electric field. The maximum energy gained in the process depends on the thickness of the shock and can be estimated to reach the MeV range at interplanetary shocks, if the shock thickness is as low as an electron skin depth (Koskinen 2011). Note that electrons will not be accelerated in this simple type of model, which has a monotonic potential (and, thus, unidirectional field) inside the shock front.

One encounter with the shock does not typically lead to a very substantial gain of energy. If, however, particles can interact with the shock many times, acceleration becomes more efficient. Shock surfing is not the only way this can happen. Particles can interact with magnetic irregularities in the plasma flow, and this can change the particle's propagation direction relative to the shock front enabling several encounters with the shock. Since particle transport under such conditions is described by diffusion relative to the local plasma flow, this acceleration mechanism is called diffusive shock acceleration (DSA) (Drury 1983; Lee 1983).

DSA can be best understood by considering shock waves propagating parallel to the magnetic field. There, as the particle crosses the shock front, its velocity vector does not change, because the magnetic field is not compressed. When the particle is moving relative to the plasma under the influence of frozen in magnetic turbulence, providing scattering centers,[1] it conserves its energy in the local plasma frame while

[1]For simplicity, the turbulence in the vicinity of the shock is often assumed to be magnetostatic, but the DSA theory can be formulated assuming that the scattering centers are propagating Alfvén waves. This simply modifies the velocities of the scattering centers.

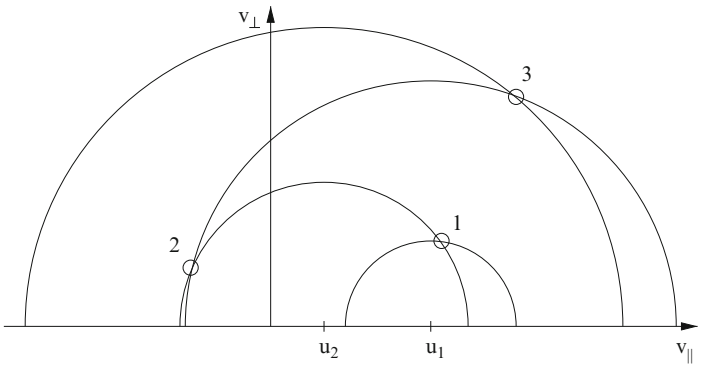

Fig. 3.5 Diffusive shock acceleration. An energetic charged particle scatters off magnetic irregularities frozen in to the local plasma flow. The numbered points depict successive crossings of the shock front, where the speed of the scattering centers changes. Because points with odd numbers must have $v_\parallel > 0$ and points with even numbers must have $v_\parallel < 0$, the shock crossings lead to a systematic gain of energy $W = \frac{1}{2}mv^2$. (From: Koskinen 2011)

simultaneously scattering in pitch angle. Upstream [downstream] particles are, thus, staying on semicircles in velocity space, centered at $(v_\parallel, v_\perp) = (u_{1[2]}, 0)$. Due to pitch-angle scattering, energetic ($v' > u$) particles can propagate in either direction relative to the shock. When the flow at the shock is compressed (i.e., $u_2 < u_1$), particles crossing the shock many times gain speed systematically as shown in Fig. 3.5.

When particle speeds are much larger than the fluid speeds, $v \gg u$, particle distributions become almost isotropic as a result of the scattering process. This enables one to calculate the energy spectrum of accelerated particles resulting from DSA. After n shock crossings, the mean particle momentum is

$$\langle p_n \rangle = p_0 \exp\left\{\frac{4}{3}\sum_{j=1}^{n}\frac{u_1 - u_2}{v_j}\right\}, \tag{3.23}$$

where $p_0 \gg mu_1$ is the injection momentum. The probability of a particle of performing at least n crossings of the shock is

$$P_n = \exp\left\{-4\sum_{j=1}^{n}\frac{u_2}{v_j}\right\} = \left(\frac{\langle p_n \rangle}{p_0}\right)^{-3u_2/(u_1-u_2)}. \tag{3.24}$$

By combing these, the integral momentum spectrum can be given as

$$N(p > \langle p_n \rangle) = N_0 \left(\frac{\langle p_n \rangle}{p_0}\right)^{-3/(r-1)}, \tag{3.25}$$

where N_0 is the total number of particles injected to the acceleration process and $r = u_1/u_2$ is the compression ratio of the shock. Thus, shock-accelerated particles have a power-law differential momentum spectrum

$$\frac{\mathrm{d}N}{\mathrm{d}p} = \frac{3N_0}{r-1}\left(\frac{p_0}{p}\right)^{(r+2)/(r-1)} \tag{3.26}$$

with spectral index $\sigma = \mathrm{d}\ln N/\mathrm{d}\ln p = (r+2)/(r-1)$ solely determined by the compression ratio of the shock. While the calculation above was presented for parallel shocks, the final result applies for oblique shocks as well.

The spectral index is actually determined by the shock's compression ratio only if $M_\mathrm{A} \gg 1$. If the Mach number of the shock is of the order unity, the magnetic scattering centers in the flow (which are actually magnetohydrodynamic waves or turbulence and not static) are no longer static magnetic fluctuations. Instead, they have non-negligible phase speeds $V_\phi \sim V_\mathrm{A}$ relative to the flow. Recall that the scattering is elastic in the frame of the propagating magnetic structure, where the electric field of the fluctuation vanishes. Taking these considerations into account when determining the *scattering-center compression ratio* of the shock (Vainio and Schlickeiser 1999), one gets

$$\sigma = \frac{r_\mathrm{sc}+2}{r_\mathrm{sc}-1}; \quad \text{with} \quad r_\mathrm{sc} = \frac{u_{1x}+V_{\phi 1}}{u_{2x}+V_{\phi 2}} \overset{M\to\infty}{\longrightarrow} \frac{u_{1x}}{u_{2x}} = r. \tag{3.27}$$

In slow-mode shocks, the scattering centers (Alfvén waves) always have larger phase speeds than fluid speeds. Thus, the scattering centers do not converge in slow shocks under many circumstances. In such cases, DSA is not operating at the shock.

Upstream of fast-mode shocks, particles can generate their own scattering centers by streaming instabilities of the Alfvén waves (Lee 1983; Afanasiev et al. 2015). This can be figured out most easily by looking at particle scattering in the upstream plasma frame. Particles conserve their energies in the frame co-moving with the MHD waves, because in that frame, the wave has no electric field (since δB has no time dependence there, as discussed above). Thus, particle energy in the plasma frame is

$$W = W' \pm V_\mathrm{A1} p'_\parallel, \tag{3.28}$$

where the signs denote waves propagating forward ($+V_\mathrm{A1}$) and backward ($-V_\mathrm{A1}$) relative to the flow. Particles entering the upstream region from downstream have $p'_\parallel/W' < -(u_1 \pm V_\mathrm{A1}) < 0$. Scatterings make the particles isotropic in the wave frame, so as a result of scatterings in the upstream region, $p'_\parallel$ increases. Thus, particle energy in the plasma frame increases (decreases) in scatterings off forward (backward) MHD waves in the upstream region. Since the total energy of particles and waves has to remain constant in the plasma frame, this means that the energy density of backward waves increases and forward waves decreases.

Finally, one should note that the power-law spectrum does not extend to infinite energies, but experiences a cut-off at some high energy determined by the age and the size of the system. Obviously, if there is limited time τ available to accelerate the particles, they cannot be accelerated beyond energies determined by $\dot{p} \sim p/\tau$, where $\dot{p}$ is the momentum gain rate related to the scattering rates and flow velocities in the system. Likewise, when the particle's diffusion length, κ/u_1, becomes of the order of the system size, the particle can not be accelerated any further, as it will not be confined to the vicinity of the shock anymore but may escape from the system. Here, $\kappa = \frac{1}{3}\lambda v$ is the spatial diffusion coefficient and λ is the scattering mean free path, which cannot be smaller than the Larmor radius of the particle. In an inhomogeneous magnetic field, such as the coronal field, particles also need to be confined by turbulence near the shock strong enough to avoid the escape by adiabatic focusing (Vainio et al. 2014). This leads to yet another condition that $\kappa/L < u_1$, where $L = -B/(\partial B/\partial s)$ is the focusing length, i.e., the scale height of the magnetic field intensity. This represents the relevant system size in the coronal medium.

3.2.4 Compressional Acceleration and Collapsing Magnetic Traps

DSA operates because of the convergence of the flow of scattering centers at the shock. The acceleration rate of an isotropic population of particles in a converging flow is given by $\dot{p} = -\frac{1}{3}p\nabla \cdot \mathbf{u}$, where $\mathbf{u}$ is the scattering center velocity. Compressional acceleration can, therefore, work also in presence of compressions ($\nabla \cdot \mathbf{u} < 0$) of non-shock type. If the diffusion length of the particles, κ/u, is much longer than the gradient scale of the flow, $L \sim u/|\nabla \cdot \mathbf{u}|$, then the compression acts on the particles as a shock, i.e., the resulting spectrum is practically the same as in the case of DSA (Jokipii and Giacalone 2007). In the opposite case, $\kappa \ll u^2/|\nabla \cdot \mathbf{u}|$, the compression will accelerate the particle distribution adiabatically. Because their diffusion length is very small, particles are primarily advected through the compression and all particles regardless of their initial momentum will gain the same factor in momentum.

Let us illustrate this with a simple example. Assume that scattering centers are frozen-in in the plasma flow. Thus, $\nabla \cdot \mathbf{u}$ is given by the hydrodynamic conservation of mass as

$$\nabla \cdot \mathbf{u} = -\frac{1}{\rho}\frac{\mathrm{d}\rho}{\mathrm{d}t}, \tag{3.29}$$

where ρ is the density of the plasma parcel being advected at velocity $\mathbf{u}$. Thus,

$$\frac{\dot{p}}{p} = -\tfrac{1}{3}\nabla \cdot \mathbf{u} = \frac{\dot{\rho}}{3\rho} \Rightarrow \frac{p^3}{\rho} = \text{constant}, \tag{3.30}$$

which is consistent with the adiabatic equation of state for a monoatomic gas, i.e., $T\rho^{-2/3} =$ constant at non-relativistic energies.

Similar to compressional acceleration, particles can be accelerated adiabatically if they are confined to a collapsing magnetic trap (see Borissov et al. 2016 and references therein). A simple example is a shrinking magnetic bottle, consisting of two magnetic mirrors in the ends, e.g., a contracting coronal loop. Particles mirroring in the ends of the trap would get accelerated, as in the rest frame of the center of the trap (the loop apex in the simple example), the mirrors in the two ends of the trap would be approaching each other. The acceleration rate is obtained from the conservation of the second adiabatic invariant, $\oint p_\parallel \mathrm{d}s_\parallel = 2|p_\parallel|s =$ constant, where the integral is along the magnetic field lines from one end of the trap to the other and back, and s is the length of the trap along the field. Decreasing s has to be compensated by increasing $|p_\parallel|$ and the parallel momentum will increase at rate

$$\frac{\mathrm{d}|p_\parallel|}{\mathrm{d}t} = -|p_\parallel|\frac{\dot{s}}{s} \tag{3.31}$$

As a magnetic bottle cannot trap particles residing in the loss-cone of the weaker magnetic mirror, this mechanism would appear at first sight to be limited to rather modest gains of momentum. However, if the magnetic field inside the trap is simultaneously increasing the betatron effect will increase the perpendicular momentum and help the particles stay trapped. The details of the magnetic configuration and its evolution will determine the acceleration efficiency of a collapsing magnetic trap.

3.2.5 Stochastic Acceleration

DSA, compressional acceleration, and collapsing traps are all examples of so-called first-order Fermi acceleration, where particles gain momentum systematically and proportionally to the speed of a moving magnetic structure. Stochastic acceleration, or second-order Fermi acceleration, is a process, where particles gain or lose energy (with a positive net energy gain) by interacting simultaneously with plasma disturbances with different phase speeds in the laboratory frame (Miller 1998). For example, if a high-energy proton is propagating in a medium with counter-propagating Alfvén waves, it can simultaneously scatter off waves propagating in both directions (Fig. 3.6, left panel). As the scatterings conserve the energy of the proton in each wave frame, the scatterings off one wave produce energy change along different characteristics in the $(v_\parallel, v_\perp)$ plane than the scatterings off the other mode. This leads to random walk of the particle in the $(v_\parallel, v_\perp)$ plane, which can be described by momentum diffusion. In this process the net momentum gain rate is proportional to the second power of the wave speed. (Hence, second-order Fermi acceleration.)

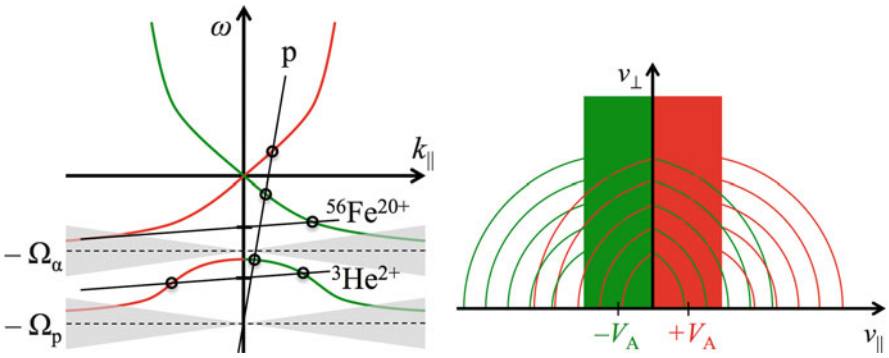

Fig. 3.6 The *left panel* shows the resonance plot for a multi-species plasma with protons and alpha particles as the major ion species. The wave modes with positive (negative) phase speeds are plotted with *green (red) curves*. The *grey shaded regions* are those where resonances with thermal ions will damp the wave power efficiently. Cyclotron waves have two branches with resonances with alpha particles and protons, respectively. The *lines* depict the resonance conditions for energetic protons ($|v\mu| \gg V_A$) and thermal minor ions. The *right panel* shows the possible velocity-space trajectories of protons in a plasma with counter propagating Alfvén waves, only. The *red (green) semicircles* are trajectories of particles interacting with Alfvén waves with positive (negative) phase speeds. The *red (green) region* depicts the velocities at which resonances with and Alfvén waves with positive (negative) phase speeds are not possible. Outside these regions, protons can always resonate with waves propagating in both directions leading to random walk in velocity space, i.e., momentum diffusion

The situation is illustrated in Fig. 3.6, right panel, where energetic protons can interact with two Alfvén waves propagating in opposite directions, when the proton velocity is situated in the region $|v_\parallel| \gtrsim 2V_A$. Scatterings off waves with positive (negative) phase speed will result in motion along the red (green) semi-circles showing that the particle energy in the plasma frame can change in a random fashion, i.e., increase or decrease. As this diffusive process spreads the distribution of protons in energy, the net effect will be acceleration. This is an example of stochastic acceleration, but other types of waves as well as randomly moving coherent structures interacting with the particles can lead to a similar situation of particles diffusing in momentum when interacting with the structures.

Figure 3.6, left panel also shows the resonant interaction of low-energy minor ions (^{3}He and iron) with higher-frequency left-handed wave modes. The figure shows that while thermal protons and alpha particles would typically resonate with heavily damped wave modes (and their resonant wave acceleration should, therefore, be somewhat inefficient), minor ions not only resonate with much less damped waves but also simultaneously with several waves propagating at different phase speeds. Especially ^{3}He can be very efficiently accelerated stochastically in this process, starting already from thermal energies. Stochastic acceleration

process, therefore, has the power to explain the peculiar abundances (strong increase in ^{3}He and heavy ion abundances over protons and alphas) observed in impulsive events (cf. Chap. 2). Note that stochastic acceleration may also occur in the turbulent sheath regions of coronal shocks and help to explain the observed double-power-law spectral form often observed in large gradual SEP events (Afanasiev et al. 2014).

3.3 Concluding Remarks

The basic acceleration mechanisms at play in erupting coronal plasmas accelerating particles to the highest energies have been described. By making several simplifications the aim has been to convey the principles of the most important SEP acceleration mechanisms, fostering efforts to create realistic and comprehensive models of solar eruptions also from the particle acceleration aspect. The models should involve realistic descriptions of both the macroscopic and microscopic fields in the plasma, as electric fields of practically all scales from the kinetic to the global may contribute to the acceleration of particles in solar eruptions.

References

Afanasiev, A., Vainio, R., Kocharov, L.: Astrophys. J. **790**, 36 (2014). doi:10.1088/0004-637X/790/1/36
Afanasiev, A., Battarbee, M., Vainio, R.: Astron. Astrophys. **584**, 81 (2015). doi:10.1051/0004-6361/201526750
Borissov, A., Neukirch, T., Threlfall, J.: Solar Phys. **291**, 1385 (2016). doi:10.1007/s11207-016-0915-0
Desai, M., Giacalone, J.: Living Rev. Sol. Phys. **13**, 3 (2016). doi:10.1007/s41116-016-0002-5
Drury, L'O.C.: Rep. Progr. Phys. **46**, 973 (1983). doi:10.1088/0034-4885/46/8/002
Isenberg, P.A.: J. Geophys. Res. **106**, 29249 (2001). doi:10.1029/2001JA000176
Jokipii, J.R., Giacalone, J.: Astrophys. J. **660**, 336 (2007). doi:10.1086/513064
Koskinen, H.: Shocks and Shock Acceleration. In: Physics of Space Storms, pp. 279–298. Springer, Heidelberg (2011)
Litvinenko, Y.E.: Astrophys. J. **462**, 997 (1996). doi:10.1086/177213
Lee, M.A.: J. Geophys. Res. **88**, 6109 (1983). doi:10.1029/JA088iA08p06109
Miller, J.A.: Space Sci. Rev. **86**, 79 (1998)
Petrosian, V.: Space Sci. Rev. **173**, 535 (2012). doi:10.1007/s11214-012-9900-6
Reames, D.V.: Solar Energetic Particles – A Modern Primer on Understanding Sources, Acceleration and Propagation. Lecture Notes in Physics, vol. 932, 127 pp. Springer, Cham (2017)
Sarris, E.T., Van Allen, J.A.: J. Geophys. Res. **79**, 4157 (1974). doi:10.1029/JA079i028p04157
Shapiro, V.D., Üçer, D.: Planet. Space Sci. **51**, 665 (2003). doi:10.1016/S0032-0633(03)00102-8

Vainio, R.: Astrophys. J. Suppl. Ser. **131**, 519 (2000). doi:10.1086/317372
Vainio, R., Schlickeiser, R.: Astron. Astrophys. **343**, 303 (1999)
Vainio, R., Pönni, A., Battarbee, M., et al.: J. Space Weather Space Clim. **4**, A08 (2014). doi:10.1051/swsc/2014005